Petroleum Science 19 (2022) 2572–2582

Contents lists available at ScienceDirect

Petroleum Science

journal homepage: www.keaipublishing.com/en/journals/petroleum-science

Original Paper

Distribution and isotopic signature of 2-alkyl-1,3,4-trimethylbenzenes in the Lower Paleozoic source rocks and oils of Tarim Basin: Implications for the oil-source correlation

Tao-Hua He [a, b, e], Wen-Hao Li [b, e, *], Shuang-Fang Lu [d, e, **], Er-Qiang Yang [a, b], Tao-Tao Jing [e], Jun-Feng Ying [b, e], Peng-Fei Zhu [b, e], Xiu-Zhe Wang [b, e], Wen-Qing Pan [c], Zhong-Hong Chen [b, e]

[a] Key Laboratory of Oil and Gas Resources and Exploration Technology, Yangtze University, Wuhan, Hubei, 430100, China
[b] School of Geosciences, China University of Petroleum (East China), Qingdao, Shandong, 266580, China
[c] Petroleum Exploration & Production Research Institute, Tarim Oilfield Company, PetroChina, Korla, Xinjiang, 841000, China
[d] Sanya Offshore Oil & Gas Research Institute, Northeast Petroleum University, Sanya, Hainan 572025, China
[e] Key Laboratory of Deep Oil and Gas, China University of Petroleum (East China), Qingdao, Shandong, 266580, China

ARTICLE INFO

Article history:
Received 28 November 2021
Received in revised form
12 March 2022
Accepted 29 July 2022
Available online 3 August 2022

Edited by Teng Zhu and Jie Hao

Keywords:
2-alkyl-1,3,4-trimethylbenzenes
Carbon isotopes
Deep lower paleozoic crude oils
Thiadiamondoid
Oil-source correlation
Tarim Basin

ABSTRACT

Series of 2-alkyl-1,3,4-trimethylbenzenes (ATMBs) were detected in most of crude oils and source rocks collected from various strata and locations of the Tarim Basin. They appeared to have heavy carbon isotopic signatures ($\delta^{13}C$, up to ~ −16‰) compared to those hydrocarbons from oxygenic phototrophic organisms, indicating that the unequivocal source of green sulfur bacteria (GSB) and photic zone euxinia (PZE) existed in the original environment. Considering the high paleoproductivity, the PZE may have enhanced the preservation of organic matter, which triggered the formation of extremely organic-rich source rocks with TOC up to 29.8% for the Lower Cambrian Yuertus Formation ($\epsilon_1 y$). The coexistence of ATMBs and the diagnostic products from secondary alterations (e.g., abundant 25-norhopanes, thiadiamondoids, and diamondoids) indicated a stronger ability of anti-second-alterations. Combined with the results of quantitatively de-convoluting mixed oil, the oil-source correlation based on ATMBs from a large number of Lower Paleozoic samples of the Tarim Basin suggested that the abundant deep crude oil resources contained a dominant contribution (>50%) from the $\epsilon_1 y$ source rocks. Therefore, the ATMBs, as diagnostic biomarkers indicating unequivocal precursors under special habitat conditions, might provide important insights for the exploration of deep Lower Paleozoic crude oils in the Tarim Basin.
© 2022 The Authors. Publishing services by Elsevier B.V. on behalf of KeAi Communications Co. Ltd. This is an open access article under the CC BY-NC-ND license (http://creativecommons.org/licenses/by-nc-nd/4.0/).

1. Introduction

Deep and/or ultra-deep strata are important targets for petroleum exploration in China (Hu et al., 2021; Li et al., 2021, 2022; Ma et al., 2022). But the high mature degree and significant secondary alterations make the oil-source correlation difficult to be carried out (Huang et al., 2016, 2017), as evidenced by the long-standing oil-source controversy in the Tarim Basin. Although the special research has lasted for more than 30 years, the oil-source problem in the Tarim Basin is still controversial (Yu et al., 2011; Huang et al., 2016; Chen et al., 2018), which is suggested by the fact that the geochemical characteristics and oil-source correlation of source rocks in the Tarim Basin are still listed as important research tasks in the National Science and Technology Major Project of China. The extraction of liquid hydrocarbon in the Well ZS1C (~6800 m) triggered a wave of deep to ultra-deep petroleum exploration in China (Sun et al., 2013; Zhu et al., 2020). And deeper industrial oil and gas production has been achieved in the Tarim Basin in the past two years (such as the most typical Well LT 1, production layer >8200 m). However, the complex multi-stage secondary alterations to steroid and terpenoid biomarkers made them ineffective at tracing the source of oil.

* Corresponding author. Key Laboratory of Deep Oil and Gas, China University of Petroleum (East China), Qingdao, Shandong, 266580, China.
** Corresponding author.
E-mail addresses: liwh@upc.edu.cn (W.-H. Li), lushuangfang@upc.edu.cn (S.-F. Lu).

https://doi.org/10.1016/j.petsci.2022.07.014
1995-8226/© 2022 The Authors. Publishing services by Elsevier B.V. on behalf of KeAi Communications Co. Ltd. This is an open access article under the CC BY-NC-ND license (http://creativecommons.org/licenses/by-nc-nd/4.0/).

Aromatic biomarkers, e.g., C_{28} triaromatic steranes (C_{28}TAS), 3-methyl-24-ethyl-triaromatic sterane (METAS), triaromatic dinosteranes (TDS) and 2-alkyl-1,3,4-trimethylbenzenes (ATMBs; these compounds were identified as 1-alkyl-2,3,6-trimethylbenzenes in several earlier publications, but according to IUPAC rules, they should be labelled as 2-alkyl-1,3,4-trimethylbenzenes, Requejo et al., 1992), have shown application potential in the study of deep oil origins (Sun et al., 2003; Huang et al., 2016; He et al., 2020a). In particular, the ATMBs indicate a special environment (photic zone euxinia:PZE) and source (green sulfur bacteria: GSB). Sun et al. (2003) reported that ATMBs were widely detected in most crude oils from the Tarim Basin, while few of them had been identified in any related Lower Paleozoic source rocks. Thus, it is very important to check the existence of ATMBs in the Lower Paleozoic source rocks so that an oil-source correlation can be carried out.

In this paper, we investigated the ATMBs in the Lower-Paleozoic crude oils and source rocks from the Tarim Basin to reveal the distribution and isotopic signature, and the effective source rocks are proposed based on an oil-source correlation.

2. Geological setting

The Tarim Basin, as a large craton basin with a remarkable buried depth of Paleozoic marine assemblage (mainly varying from 6000 to 12000 m), is the most petroliferous province with abundant deep petroleum resources in China. It covers a total area of 5.6×10^5 km^2. This basin has four uplifts and five depressions structures on first-order tectonic units, including the Northern, Southeast, Southwest, Tanggu, and Kuche Depressions, Bachu, Tazhong, Tabei, and Tadong Uplifts, respectively (Liu et al., 2016; He et al., 2022a).

During the geological history, frequent orogenies triggered 18 recognized unconformities in the basin (Cai et al., 2009), which provided migration paths and accumulation sites for the deep crude oil. These oils underwent severe secondary alterations and varied dramatically from condensate, light oil, normal oil, waxy oil and heavy oil to solid bitumen, resulting in a decades-long controversy over their origin (Cai et al., 2015; Zhan et al., 2016; Huang et al., 2016, 2017; Zhu et al., 2018a; Wang et al., 2020). The main source for Lower-Paleozoic crude oils was indicated to be Cambrian-Lower Ordovician ($\in$-O_1) and/or Middle-Upper Ordovician ($O_{2\text{-}3}$) strata (He et al., 2020a). While numerous studies suggested that the Upper Ordovician Lianglitage Formation (O_3l), as the potential source rock from $O_{2\text{-}3}$ strata, was only distributed in the Tazhong Uplift and had lower total organic carbon (TOC) content, indicating that it is not likely to form large-scale deep oil resources in the Tazhong and Tabei Uplifts (Huang et al., 2016). Recently, Zhu et al. (2018b) reported another potential source rock from the Lower Cambrian Formation source rocks ($\in_1y$) covering a thickness of 10–15 m and an area of 2.6×10^5 km^2, which was thought to be the major source rock that had made remarkable contributions to the current abundant Lower-Paleozoic crude oil resources. And during the development of this set of source rocks, as described in our previous works (He et al., 2020b, 2022a), abundant nutrients from continental weathering and frequent hydrothermal activities promoted the bloom of plankton, resulting in the significant enrichment of TOC (up to 29.8%) in the $\in_1y$ shale (Zhu et al., 2021). Additionally, the hydrothermal activity brought hydrogen sulfide (H_2S) into the ocean, which triggered anoxic conditions or H_2S poisoning environments (Zhou et al., 2014; He et al., 2020b). This benthic condition was not conducive to the survival of benthos that were generally hydrogen-poor and did not tend to generate oil; however, it is conducive to the preservation of organic matter from the plankton organisms that boomed in the photic zone, which were generally hydrogen-rich and tended to generate oil (Peters et al., 2005; Zhang et al., 2016; He et al., 2020b).

ATMBs were firstly detected in most oils from the Tarim Basin, while few of them were identified in any Lower Paleozoic source rocks for several years, indicating that the unknown source rocks with ATMBs must have been developed in this basin (Sun et al., 2003). In recent years, with the increase in the number of exploration wells and the number of field outcrops, source rocks with abundant ATMBs have been gradually discovered in this and previous studies (He et al., 2022a). However, further related research in the Tarim Basin is still very limited.

3. Samples and experiments

3.1. Samples

A set of 115 potential source rock samples were collected from the Tarim Basin (Chen et al., 2018; He et al., 2020a, b, 2022a, b), including 91 core samples from the Tazhong Uplift (Well TZ12 and TZ30), Tabei Uplift (Well XH1, QT1, LT1, LT3 and LN46) and Tadong Uplift (Well ML1 and TD2), and 24 outcrop samples from the Shenairike (SARK) section in the northwestern Tarim Basin, and Queerqueke (QEQK) section in the northeastern Tarim Basin. These samples covered almost all the lithology, including black shale, mudstone, siliceous rock, argillaceous limestone, and limestone; and strata from the Cambrian-Ordovician, including the Lower Cambrian Yuertus Formation ($\in_1y$), Middle-Lower Ordovician Heituao Formation ($O_{1\text{-}2}h$), Middle-Upper Ordovician Salgan Formation ($O_{2\text{-}3}s$), and O_3l, respectively. Besides, we also sampled 35 marine crude oil samples from oil production wells in the Tarim Basin (Table 1). These crude oil samples covered the age of Carboniferous (C), Devonian (D), Silurian (S), Ordovician (O) and Cambrian ($\in$). The properties of crude oil were distributed from light condensate (such as ZS1C, the buried depth of the production layer is 6861.00–6944.00 m) to heavy biodegraded oil (such as well RP4C, the production layer is 6918.42–7026.12 m), in which light oil accounted for about 69% and heavy oil accounted for about 31%. To make the results more reliable, we employed sufficient amount of sample to be analyzed, which covered most of the reservoir developed under different structural zones, different buried depths and different properties in the Tarim Basin. Among them, it was summarized in a review work that the crude oil from the Well YM2 (3598–6050 m, O_3l) represented the end-member oil from $O_{2\text{-}3}$ source rocks and the crude oil from the Well TD2 (4562–5040 m, $\in$) represented the end-member oil from the Cambrian-Lower Ordovician source rocks (Huang et al., 2016).

3.2. Experiments

The fine-ground (<100 mesh) source rock samples were Soxhlet extracted for 72 h using a mixture of methanol: dichloromethane (DCM) (7:93 v:v; He et al., 2018). Asphaltenes of extracts and oil samples (~50 mg) were precipitated by moderate light petroleum ether equal with 50 times volume to that of the sample followed by filtration. The filtrate was further separated by liquid chromatography on a silica gel-alumina column by using light petroleum ether to elute the saturated fraction, DCM to elute the aromatic fraction and a mixture of methanol: chloroform (3:97 v:v) to elute the resins. Aromatic fractions were analyzed on an Agilent 6890N-Agilent 5973N gas chromatography-mass spectrometry (GC-MS) equipped with an Equity-5 capillary column (60 m length, 0.25 mm i.D., 0.25 μm film thickness). The GC oven temperature was initially kept at 50 °C for 2 min, then programmed to 200 °C at a rate of 3 °C/min, then programmed to 320 °C at a rate of 10 °C/min with an isothermal holding for 20 min. Full-scan detection and selective ion

Table 1
Information of typical marine oil samples in the Tarim Basin.

IM	Well number	Top depth, m	Bottom depth, m	Strata	Structural location
C01	Ln631	5800.81	5845.00	O_2y	Tabei Area
C02	Ma4	1800.34	2041.20	$C_1b + O_2y$	STBA
C03	Xk7C	6900.00	6930.00	Oy	Tabei Area
C04	Tz83	5433.00	5441.00	O_3l	Tazhong Area
C05	Ym204	5845.00	5920.50	O_2y	Tabei Area
C06	Tz40	4306.00	4340.00	Cd	Tazhong Area
C07	Ma3	1508.00	1518.00	O_3l	STBA
C08	Ha6	5953.00	5954.00	C	Tabei Area
C09	Tz62	4700.50	4758.00	O_3l	Tazhong Area
C10	Ym102	7249.03	7313.00	O_3l	Tabei Area
C11	RP4C	6918.42	7026.12	O_3l	Tabei Area
C12	JY5H	7043.00	7255.00	$O_{2\text{-}3}y$	Tabei Area
C13	Zg2	5866.00	5893.00	O_3l	Tazhong Area
C14	Rp301	7006.00	7069.00	O_2y	Tabei Area
C15	Ma3	1414.00	1424.00	Cb	STBA
C16	Ls2	5741.00	5830.00	O_1p	STBA
C17	Tz72	5428.00	5561.73	O_3l	Tazhong Area
C18	Zs1C	6861.00	6944.00	ϵ_1x	Tazhong Area
C19	Qun6	5507.69	5588.69	D_3d	STBA
C20	Tz10	4616.32	5350.00	S_1t- S_1k	Tazhong Area
C21	Tz62	4052.88	4075.58	S_1t	Tazhong Area
C22	Tz12	4339.50	4413.50	S_1k	Tazhong Area
C23	Zg43	4800.00	5334.09	O_1y	Tazhong Area
C24	Ma4	2018.00	2022.00	O_2y	STBA
C25	Tz103	3743.00	3746.00	D_3d	Tazhong Area
C26	Ma8	1488.56	1569.21	C_1b	STBA
C27	Tz1	3659.00	3684.00	ϵ	Tazhong Area
C28	Ym2	3597.68	6050.00	O	Tabei Area
C29	Yg2	6041.00	6125.00	O	Tabei Area
C30	Tz10	4206.00	4230.00	Cd	Tazhong Area
C31	Rp3	6977.20	7040.00	O_2y	Tabei Area
C32	Zs1	6426.00	6497.00	ϵ_2a	Tazhong Area
C33	Jy1	7154.61	7208.40	O_2y	Tabei Area
C34	Tz1	3659.00	3684.00	O	Tazhong Area
C35	Ln62	5565.00	5578.00	D_3d	Tabei Area

Note: IM, Identification mark of crude oil sample; STBA, Southwest Tarim Basin area (He et al., 2022b).

monitoring (SIM) were performed. The selected ions for ATMBs detection were *m/z* 133 and 134.

Compound-specific $\delta^{13}C$ of ATMBs were measured on several typical crude oil samples using the two-step method that was implied for separation and concentration of ATMBs. The first step is to obtain the monoaromatic fraction. Fill the bottom of the chromatographic column with an appropriate amount of absorbent cotton, first add 2 g chromatographic silica gel, then add 2 g neutral alumina. Gently tap the chromatographic column to fill the stationary phase evenly, and immediately add an appropriate amount of petroleum ether to wet the chromatographic column. When the liquid level of petroleum ether is close to the top interface of the neutral alumina stationary phase, drop the oil sample (~50 mg) into the chromatographic column. When the liquid level of the sample is close to the top interface of the stationary phase, 30 ml of petroleum ether was used to remove the saturated hydrocarbon, and another 6 ml of mixed solvents of petroleum ether/dichloromethane of 99:1 (v:v) was added to elute to obtain the monoaromatic fraction. The second step is to concentrate the ATMBs. The concentrated monoaromatic fractions were first eluted over silica gel with cyclohexane to remove linear alkylbenzenes, and then over-activated alumina with hexane and hexane/DCM (9:1 v:v). Notably, alumina needs to be activated under ~145 °C for 4 h before being used, and all filtrates should be air-dried naturally rather than accelerated by nitrogen purging. Otherwise, the small molecular targets might be evaporated. The final product is relatively enriched in ATMBs, which was checked by the comparison of total ions chromatogram (TIC) and selective scanning (*m/z*=134) diagrams (Suppl. Fig. S1). Finally, compound-specific $\delta^{13}C$ analysis of ATMB fractions was performed on the Finnigan^{PLUS} XL IRMS interfaced to an HP6890 GC by a combustion III interface, including a J&W DB5 column (50 m length, 0.32 mm i.D., 0.25 μm film thickness). The GC oven temperature program was initially held for 5 min at 35 °C, heated up to 140 °C at 2 °C/min, then from 140 °C to 290 °C at 20 °C/min, and finally held for 30 min at 290 °C.

The 2-thiadiamondoids in crude oils were measured on a Micromass Platform II spectrometer coupled to a Hewlett-Packard 6890 GC, including an HP-5MS column (30 m length, 0.25 mm i.D., 0.25 μm film thickness). The GC oven temperature program was initially held for 2 min at 60 °C, then heated from 60 °C to 315 °C at 3 °C/min, and finally held for 15 min at 315 °C. The detail process was reported by Xiao et al. (2019).

4. Results

4.1. Biomarkers

Maturity related parameters TNR-3 (TNR-3 = 1,3,7-/(1,3,7-+1,2,5-) trimethylnaphthalenes) of extractions appeared to be>0.4 and TeNR values (TeNR=1,3,6,7-/(1,3,6,7-+1,2,5,6-+1,2,3,5-) tetramethylnaphthalenes) are >0.4 (Table 2). These values indicate the Cambrian-Ordovician source rocks were mainly under the high mature stage. Similarly, crude oils were at a high mature stage and most of them were products of source rocks under a high maturity stage. With this mature-high mature condition, there were large overlaps in traditional biomarker (steranes and terpanes) parameters susceptible to maturity, such as Pr/Ph, C_{23}/C_{21} tricyclic terpanes (TT), 4-MSI (4-methylsterane index = 4-methylsteranes/

Table 2
Geochemical parameters calculated from source rocks and crude oils in the Tarim Basin.

IM	a	b	c	d	e	f	g	h	i	j	k	l	m	n
S−O_3l*	0.77-1.05/0.92***	0.70-1.63/1.32	0.81-1.83/1.44	0.01-0.05/0.02	22-41/33	20-32/26	29-53/41	50-64/58	0.21-0.51/0.35	0.13-0.24/0.17	0.10-0.24/0.15	0.13-0.81/0.41	0.45-0.82/0.60	0.48-0.84/0.60
S−$O_{2-3}s$	1.07-1.96/1.23	0.38-0.67/0.54	0.78-2.29/1.45	0.24-1.07/0.68	33-45/38	19-32/27	27-45/36	29-48/39	0.79-0.95/0.87	0.57-1.12/0.88	0.44-0.74/0.59	0.41-0.88/0.81	0.69-0.75/0.72	0.66-0.74/0.70
S−$O_{1-2}h$	0.72-1.15/0.86	0.49-0.96/0.49	0.73-2.49/1.24	0.49-0.81/0.62	27-57/42	21-36/26	21-47/35	37-52/42	0.71-0.78/0.75	0.59-1.01/0.80	0.31-0.69/0.42	1.43−74.53/16.28	0.45−85/0.63	0.49-0.73/0.64
S-$Є_1y$	0.55-0.95/0.57	0.42-0.74/0.51	0.58-2.04/1.41	0.41-0.70/0.55	36-52/44	21-29/25	27-38/35	36-47/44	0.66-0.85/0.76	0.48-1.19/0.81	0.37-0.64/0.46	1.13−164.24/19.85	0.41-0.90/0.59	0.41-0.90/0.61
C01**	0.70	0.71	2.04	0.36	42	27	32	0.49	0.70	0.48	0.38	17.13	0.79	0.79
C02	1.86	1.07	0.71	0.18	27	29	43	0.49	0.79	0.78	0.45	0.25	0.79	0.67
C03	0.72	0.64	2.03	/	36	22	42	0.76	0.11	0.42	0.08	7.50	0.77	0.85
C04	0.78	0.88	2.07	0.95	38	30	32	0.76	0.11	0.54	0.11	11.92	0.82	0.87
C05	0.82	0.99	1.90	/	30	20	49	0.78	0.11	0.27	0.07	11.14	0.66	0.69
C06	0.82	0.78	1.96	/	35	22	43	0.71	0.16	0.31	0.14	12.29	0.66	0.67
C07	1.34	0.59	0.71	0.41	35	31	35	0.43	0.82	1.47	0.41	0.81	0.69	0.67
C08	0.73	0.56	1.90	0.05	34	24	42	0.71	0.22	0.54	0.14	9.86	0.64	0.71
C09	0.70	0.63	1.55	0.15	29	29	42	0.70	0.32	0.69	0.10	17.34	0.73	0.74
C10	0.71	0.56	1.99	/	34	23	43	0.38	0.85	/	0.72	12.08	0.93	0.97
C11	0.72	0.78	2.04	/	37	20	43	0.74	0.33	0.29	0.12	15.05	0.76	0.80
C12	0.75	0.75	2.02	/	30	22	47	0.69	0.12	0.39	0.14	9.34	0.79	0.89
C13	0.86	0.48	1.39	/	54	17	29	0.49	0.20	/	0.44	19.73	0.81	0.85
C14	0.78	0.66	1.83	/	44	18	38	0.66	0.18	/	0.22	36.98	0.84	0.89
C15	1.80	0.59	0.87	0.55	34	32	34	0.40	0.87	2.09	0.55	0.40	0.61	0.59
C16	0.81	0.67	1.87	/	39	22	40	0.48	/	0.50	0.33	72.81	0.64	0.68
C17	0.95	0.63	0.83	/	31	26	43	0.55	0.13	/	0.42	72.78	0.64	0.68
C18	0.78	/	/	/	/	/	/	0.46	0.85	/	0.61	1505.58	0.95	0.98
C19	1.26	/	2.31	/	/	/	/	0.69	0.14	/	0.16	3.63	0.79	0.80
C20	0.74	0.78	1.88	/	34	22	45	0.73	0.10	0.33	0.12	16.25	0.63	0.65
C21	0.97	0.66	0.96	0.22	31	34	35	0.45	0.55	1.09	0.59	1.58	0.74	0.77
C22	0.69	0.55	2.10	/	31	22	47	0.72	0.03	0.37	0.16	21.67	0.52	0.58
C23	0.68	2.34	1.84	/	29	26	45	0.74	0.14	0.52	0.10	6.59	0.74	0.79
C24	1.38	/	0.78	/	36	27	36	0.58	0.85	0.00	0.31	1.85	0.59	0.53
C25	0.63	0.47	1.50	/	38	27	36	0.72	0.12	0.42	0.09	51.08	0.81	0.78
C26	1.20	/	/	/	/	/	/	0.41	0.85	/	0.46	1.98	0.85	0.72
C27	0.65	0.59	1.51	/	32	27	41	0.73	0.15	0.70	0.09	32.09	0.73	0.72
C28	0.63	0.94	1.94	/	32	23	45	0.77	0.13	0.31	0.08	12.80	0.69	0.71
C29	1.20	0.78	1.28	/	38	14	48	0.46	0.22	0.40	0.57	11.79	0.79	0.86
C30	0.66	0.70	1.85	0.30	29	30	41	0.71	0.26	0.79	0.15	3.30	0.67	0.65
C31	0.67	0.72	1.83	0.09	41	20	39	0.75	0.09	0.31	0.11	28.99	0.85	0.88
C32	0.67	0.67	1.65	/	40	23	37	0.69	0.22	0.32	0.18	38.70	0.93	0.91
C33	0.68	0.74	1.97	/	37	21	42	0.63	0.24	0.33	0.23	15.10	0.86	0.92
C34	0.67	0.58	1.48	/	31	28	42	0.75	0.12	0.54	0.07	28.82	0.75	0.73
C35	0.63	0.63	1.86	0.69	38	29	33	0.44	0.80	1.22	0.51	6.90	0.69	0.61

Note: IM, Identification mark; S−O_3l*, source rocks from the O_3l; C01**, crude oil-01; ***, min-max/average; a, Pr/Ph; b, $C_{24}Tet/C_{26}TT$; c, $C_{23}TT/C_{21}TT$; d, 4-MSI = 4-methylsteranes/$\alpha\alpha\alpha C_{29}$ regular sterane (C_{29} St); e, C_{27} St % = C_{27} St/(C_{27} St + C_{28} St + C_{29} St)*100%; f, C_{28} St % = C_{28} St/(C_{27} St + C_{28} St + C_{29} St)*100%; g, C_{29} St % = C_{29} St/(C_{27} St + C_{28} St + C_{29} St)*100%; h, C_{28} TAS % = C_{28} TAS/C_{26-28} TAS; i, TDSI = TDS/(TDSs + METASs); j, G/C_{31}HR; k, $C_{26}S/C_{28}S$ TAS; l, SF/OF; m, TeNR = 1,3,6,7-/(1,3,6,7- + 1,2,5,6- + 1,2,3,5-) tetramethylnaphthalenes; n, TNR-3 = 1,3,7-/(1,3,7- + 1,2,5-) trimethylnaphthalenes (Peters et al., 2005).

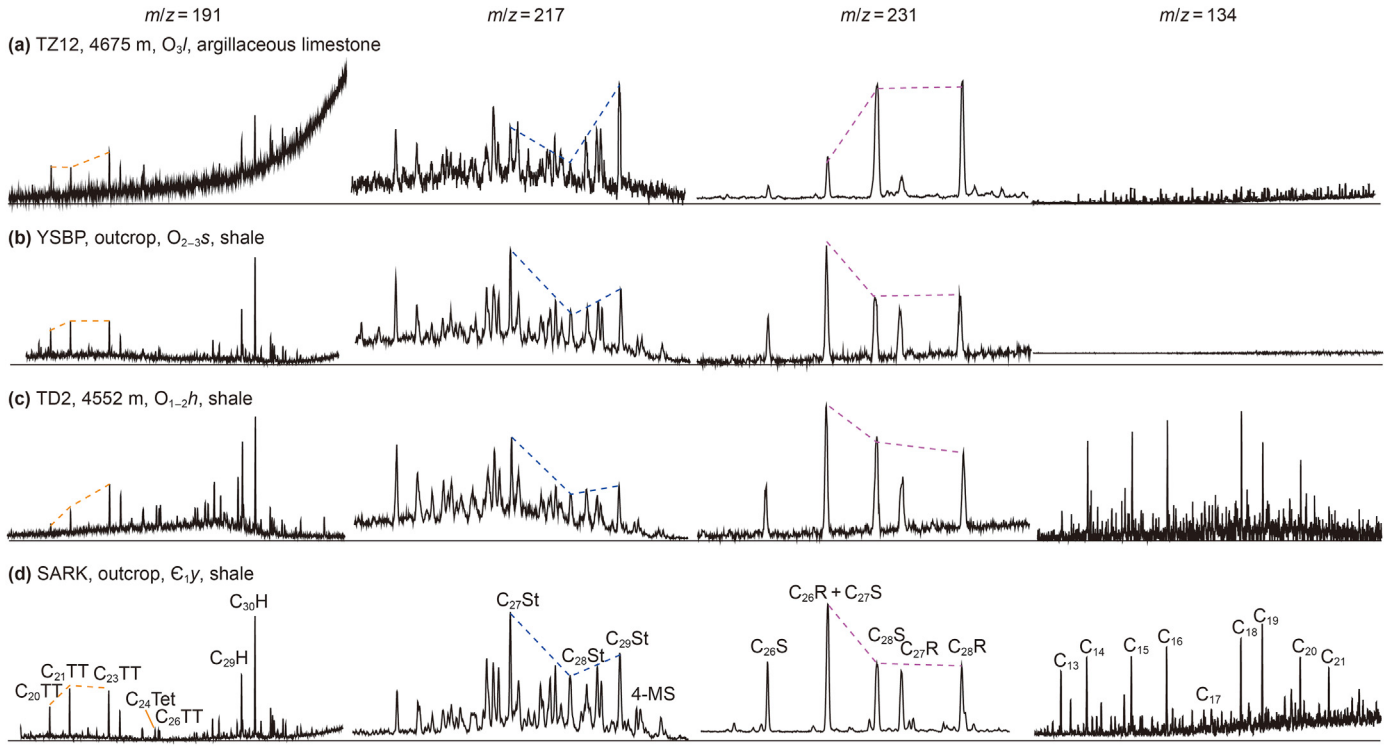


Fig. 1. The distributions of terpanes ($m/z = 191$), steranes ($m/z = 217$), triaryl steranes ($m/z = 231$) and ATMBs ($m/z = 134$) in typical Cambrian-Ordovician source rock samples from the Tarim Basin (TT, tricyclic terpane; C_{27} St, $\alpha\alpha\alpha C_{27}$ regular sterane; C_{28} St, $\alpha\alpha\alpha C_{28}$ regular sterane; C_{29} St, $\alpha\alpha\alpha C_{29}$ regular sterane; $C_{26}S$, $C_{26}S$ triaryl steranes; C_{13}, ATMB- C_{13}).

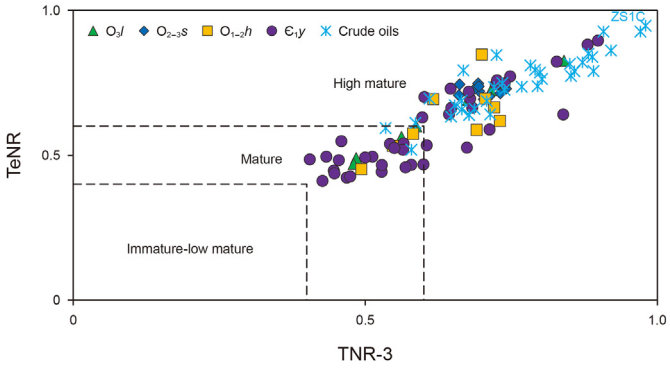


Fig. 2. Thermal evolution degree of Cambrian-Ordovician source rocks and crude oils in the Tarim Basin (TNR-3 = 1,3,7-/(1,3,7-+1,2,5-) trimethylnaphthalenes; TeNR = 1,3,6,7-/(1,3,6,7-+1,2,5,6-+ 1,2,3,5-) tetramethylnaphthalenes; Peters et al., 2005).

$\alpha\alpha\alpha C_{29}$ regular sterane (C_{29} St)), relative percentage content of C_{27} St, C_{28} St, and C_{29} St (Fig. 1). Even the above biomarkers were destroyed at a higher degree of thermal evolution, such as the crude oil from the well ZS1C with TeNR of 0.95 and TNR-3 of 0.98 (Table 2, Fig. 2). It is noteworthy that extraction from the $O_{2-3}s$ source rocks showed a "V" shaped distribution of C_{27}-C_{29} St with a dominant abundance of C_{27} St, an "L" shaped distribution of $C_{26}R$+$C_{27}S$ TAS-$C_{28}S$ TAS-$C_{28}R$ TAS with a lower abundance of C_{28} TAS, as well as a relatively significant distribution of 4-methylsterane and gammacerane (Fig. 1), which were believed to be the identification marks of Cambrian source rocks, while opposite to that of Ordovician source rocks (Huang et al., 2016). It means that previous classification schemes based on traditional biomarkers could not reflect the real differences among the Cambrian-Ordovician source rocks.

The $m/z = 134$ aromatic fractions chromatogram of partial extracts and all crude oils displayed completely distributed peaks of ATMBs with varying carbon numbers from 12 to 22 (Fig. 1 and Suppl. Fig. S2). The mass spectra of them were characterized by a base peak at m/z 133/134, molecular ion peak at m/z 147+14n (n = 1–12) and other corresponding characteristic peaks at m/z 91/105/119/147/147 + 14n, which was consistent with the general formula of C_nH_{2n-6} of a trimethylbenzene series (Suppl. Fig. S2d-e). Furthermore, with the increasing carbon number of ATMBs (ATMB-C_i, $i = 12–22$), the regular absence or low value occurred at ATMB-C_{23}, ATMB-C_{17}, and ATMB-C_{12} (Suppl. Figs. S2a–c). And the predominance of ATMB-C_{13}~C_{16} and ATMB-C_{18}~C_{22} homologues could be observed. They were consistent with the mass spectra of irregular isoprenoids containing a tail-to-tail linkage (Lu et al., 2015) and thus were considered as side chains of ATMBs. The mass spectrum and retention time of them were further compared with the published standard (Summons and Powell, 1987; Requejo et al., 1992; Sun et al., 2003). It was believed that the observed ATMBs were 1,3,4-trimethyl-aryl isoprenoids according to IUPAC rules (Requejo et al., 1992).

The 2-thiaadamantanes were only detected in five crude oils with a wide-varying concentration difference, from 30 μg/g oil to 8578 μg/g oil, indicating that most of crude oils have not been altered by thermochemical sulfate reduction (TSR) (Wei et al., 2012). Furthermore, the highest 2-thiadiamondoids content of 8578 μg/g oil occurred in the crude oil from the well ZS1C (6861–6944 m, Є, 165 °C, 74–75 MPa).

4.2. Compound specific $\delta^{13}C$ of ATMBs

Compound specific $\delta^{13}C$ of ATMBs ranged from −26.42‰ to −16.17‰ (Table 3), which were 8‰–15‰ heavier than lipids of algae or other bacteria (Table 4). The average compound-specific $\delta^{13}C$ of ATMBs of each sample was about −20‰, indicating that ATMBs from these samples had the same precursors.

Table 3
Compound specific $\delta^{13}C$ (‰) compositions of ATMB from typical crude oils.

Wells	HD23	Ha6	TZ11	YM2-8	YM2-14
Depth, m	5953–5954	4301–4307	6253–6440	5773–5900	5775.5–5915
ATMB-C_{13}	−21.10*	−18.61	−18.28	−19.11	−17.40
ATMB-C_{14}	−17.00	−17.00	−18.33	−17.39	−18.00
ATMB-C_{15}	−20.16	−19.49	−16.61	−22.48	−19.30
ATMB-C_{16}	−19.44	−18.55	−18.72	−25.97	−20.24
ATMB-C_{17}	−18.33	−19.22	−24.98	−19.11	−19.70
ATMB-C_{18}	−18.33	−17.00	−18.44	−16.17	−17.70
ATMB-C_{19}	−19.72	−18.39	−24.59	−26.42	−18.50
ATMB-C_{20}	−21.38	−21.54	−20.71	−23.04	−20.36
ATMB-C_{21}	−24.42	−20.05	−26.42	−24.87	−23.54

Note: *, the $\delta^{13}C$ of ATMB with 13 carbons from the oil in Well HD23 (5953–5954 m) was −21.10‰.

Table 4
Compound specific $\delta^{13}C$ of ATMBs derived from GSB.

Compounds* (ATMBs)	$\delta^{13}C$	Differentiation**	Literature
ATMB-C_{15}, C_{18-21}	−24.7 ~ −21.6‰	8‰	Summons and Powell (1986)
ATMBs	−19 ~ −14‰	12–16‰	Hartgers et al. (1994a), b
ATMB-C_{13-15}	−17.7 ~ −15.6‰	12–15‰	Grice et al. (1997)
ATMB-C_{16}	−19‰	15‰	Koopmans et al. (1996a)
TTMBs	−16.8 ~ −15.5‰	14‰	Pedentchouk et al. (2004)
ATMBs	−24.87 ~ −16.17‰	8–15‰	this study

Note: GSB, green sulfur bacteria; TTMB, 1,2,3,4-tetramethylbenzene derived from GSB; *, ATMBs or ATMBs with specific carbon number; **, average difference of $\delta^{13}C$ values between ATMB or TTMB and compounds from lipids of algae or other bacteria.

5. Discussions

5.1. Distribution of ATMBs

ATMBs have been identified for the first time by Summons and Powell (1987) and they have been consequently detected in crude oils worldwidely (Sun et al., 2003; Grice et al., 2005; Lu et al., 2015; He et al., 2022a). The ATMBs detected in this work had characteristic fragment ions at *m/z* 134 or 133 and contained a trimethylalkyl-aryl structure, which could be easily observed on the mass chromatograms of *m/z* 134 or 133 (Summons and Powell, 1987). The mass chromatograms of *m/z* 134 or 133 also have been performed on possible source rock samples, but the peaks of ATMBs in the aromatic fractions were only observed in the $O_{1\text{-}2}h$ and $\epsilon_1 y$ source rocks. It indicated that the ATMBs, as specific biomarkers, might have a special precursor and be only developed under the photic anoxic zone (Peters et al., 2005). Because the $O_{2\text{-}3}s$ source rocks were developed under the anoxic environment in platform depression, the $O_3 l$ source rocks were developed under a weak reduction environment in the platform, while the $O_{1\text{-}2}h$ and $\epsilon_1 y$ source rocks were developed under an anoxic-euxinic condition in the slope or basin (Huang et al., 2016; He et al., 2020b, 2022a). In sharp contrast, they were identified in all crude oils, including condensate, light oil, normal oil, waxy oil to heavy oil.

It was summarized that with the increase of thermal maturity, some traditional biomarkers, such as isoprenoids, steranes, and terpanes widely used for oil-source correlation, might lose their original significance and were hardly used for oil-source correlations (Peters et al., 2005). Moreover, secondary alterations have been widely reported in the Tarim Basin, especially thermal alteration, biodegradation, and TSR.

The comparison of the same set of source rocks ($\epsilon_1 y$) under different degrees of thermal evolution showed that the ATMBs could still be completely generated even under a high degree of thermal stage (EqR_o = 1.5% ~ > 2.0%), indicating the high thermal stability of ATMBs. The notable difference may be reflected in the thermal stability of high-carbon-number ATMBs (>ATMB-C_{17}) and low-carbon-number ATMBs (<ATMB-C_{17}). The relative content of high-carbon-number ATMBs was significantly higher than or similar to that of low-carbon-number ATMBs for source rocks under high maturity stage (EqR_o = 1.3–2.0%), such as those from the Well ML1 (EqR_o ~ 1.8%) in the Tadong Uplift and the Well LT1 (EqR_o = 1.5–1.7%) in the Tabei Uplift (Suppl. Fig. S2ab). The relative abundance of high-carbon-number ATMBs was significantly lower than that of low-carbon-number ATMBs for source rocks with post maturity degree (EqR_o > 2.0%), such as those from the Well TD2 (EqR_o > 2.0%) in the Tadong Uplift (Suppl. Fig. S2c). In the present study, the ATMBs from normal crude oils and heavy crude oils had a bimodal distribution (dominant ATMB-C_{18} ~ ATMB-C_{22} and ATMB-C_{13} ~ ATMB-C_{16}) or a post-peak distribution (dominanted by ATMB-C_{18} ~ ATMB-C_{22}), while those from light crude oils and condensate only held the front-peak distribution (dominanted by ATMB-C_{13} ~ ATMB-C_{16}). This indicated that the high-carbon-number ATMBs tended to decrease and the distribution pattern might change from bimodal distribution or post-peak distribution to front-peak distribution with the increase of maturity, which was consistent with the published result (Requejo et al., 1992). Additionally, these $\epsilon_1 y$ source rocks with abundant ATMBs had Pr/Ph ratios <1.0, indicating that ATMBs were mainly developed under anoxic conditions (Peters et al., 2005).

Moreover, the complete distribution of ATMBs was identified in the biodegraded crude oils that contained abundant biodegradation products, e.g., abundant 25-norhopanes in the sample of oil C04 (well Tz83, 5433–5441 m, $O_3 l$) in the Tazhong Uplift (Fig. 3). The crude oil of C04 was thought to be a mixed oil having the source rocks of Cambrian (namely $\epsilon_1 y$) and $O_3 l$, but during the biodegradation process (Late Ordovician), the Cambrian source rocks were under a mature stage (oil-generation peak) while the $O_3 l$ source rocks were under immature stage (no oil generated) (Sun et al., 2003; Liu et al., 2021). Furthermore, the crude oil of C04 showed the high C_{28} TAS abundance and low $C_{26}S/C_{28}S$ TAS ratio characteristics of $O_3 l$ source rocks. This suggested that this crude oil contained the early filled crude oil from Cambrian source rocks and the late filled crude oil from $O_3 l$ source rocks. And the early filled

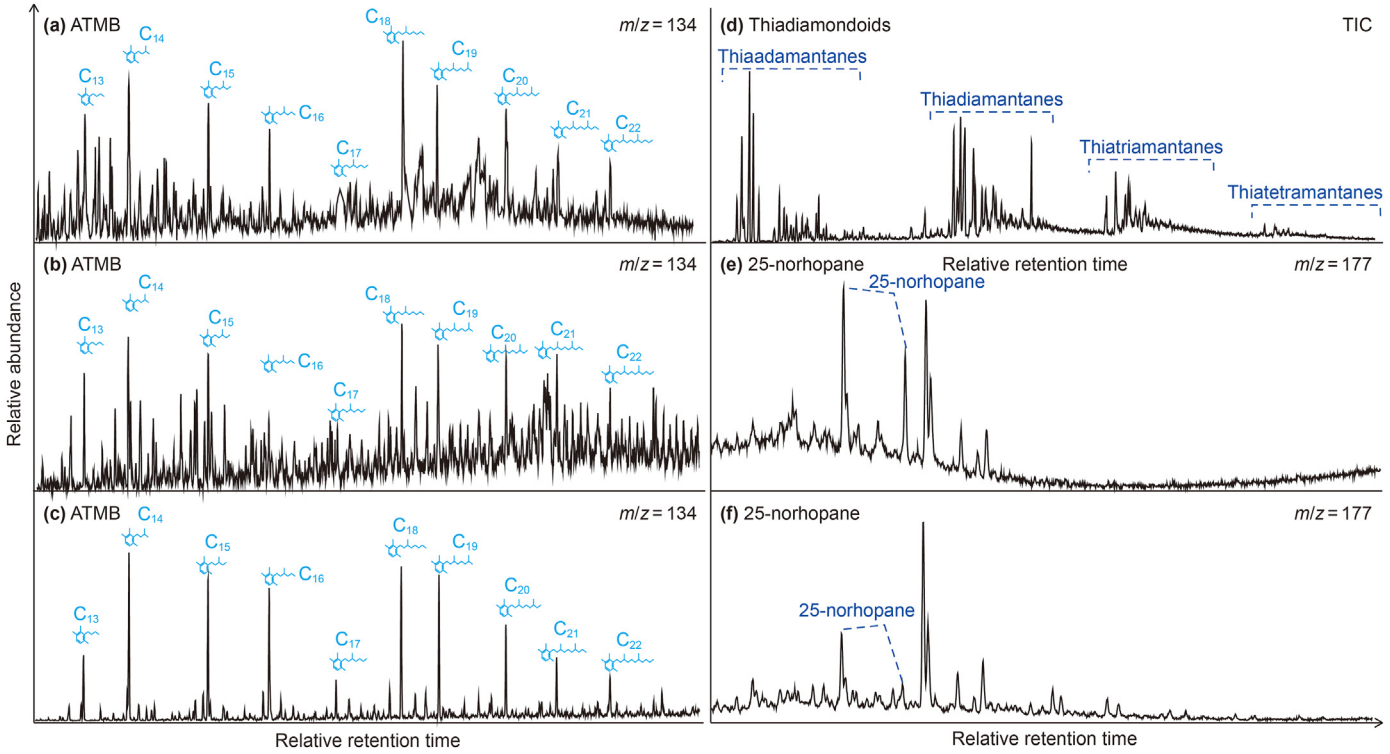


Fig. 3. Mass chromatograms of ATMB, thiadiamondoids and 25-norhopane in crude oils (Note: a, d, crude oil from the well ZS1C (6861–6944 m); b, e, crude oil from the well Tz83 (5433–5441 m, O_3l); c, f, a reference crude oil from the well Ym2 (3597.68–6050 m, O)).

crude oil was severely biodegraded before the late filled crude oil arrived. The distribution of ATMBs from this crude oil displayed no obvious difference from that of normal crude oil (Fig. 3b). As a result, ATMBs in this crude oil were only derived from $\epsilon_1 y$ source rocks, indicating that ATMBs have experienced biodegradation process and retained. Thus, ATMBs have a strong ability to resist anti-biodegradation.

A similar observation of ATMBs occurred in crude oils that suffered severer TSR. Most commonly, the crude oil C18 (well ZS1C, 6861–6944 m, ϵ, 165 °C, 74–75 MPa) was condensate from the lower Cambrian, with a density of 0.79 g/cm^3, a sulfur content of 2.06%, higher 2-thiadiamondoids content of 8578 μg/g oil, diamondoids content of 155000 μg/g oil, dibenzothiophenes content of 70 mg/g oil (Ma et al., 2018). In terms of specific characteristics, these diamondoids detected in the saturate fraction contained higher diamondoids, including tetramantanes, pentamantanes, hexamantanes, and cyclohexamantane, which were products of strong thermal alteration; additionally, higher thiadiamondoids (Fig. 3d) and diamondoidthiols, including thiatetramantanes, tetramantanethiols, thiapentamantanes, and pentamantanethiols, were also detected in the OSC fraction. As a molecular fingerprint of TSR, thiadiamondoids with high abundance revealed that this crude oil had suffered extreme-TSR and strong-thermal alterations (Ma et al., 2018; Jiang et al., 2008), which was also supported by the sulfur isotope ($\delta^{34}S$) of specific compounds (Cai et al., 2016). The detection of ATMBs in this oil could (Fig. 3a) suggest that the ATMBs had strong anti-thermal alteration and anti-TSR alteration abilities.

5.2. Isotopic signature of ATMBs

The ATMBs were thought to be possible products after geological transformation from aromatic carotenoids (isorenieratene, renieratene, chlorobactene, renierapurpurine, and okenone) (Brocks and Schaeffer, 2008). These aromatic carotenoids could be derived from a variety of precursors, including algae, photosynthetic purple sulfur bacteria and GSB. But the isorenieratene, one of the aromatic carotenoids, was identified as a carotenoid uniquely biosynthesized by GSB with a much heavier compound-specific $\delta^{13}C$ (Sinninghe Damsté et al., 2001), due to the GSB adopting a unique way, a reverse tricarboxylic acid cycle, to fix CO_2, which led to an anomalously enriched ^{13}C in the synthetic organic matter, including the organic organism (Quandt et al., 1977). While other precursors, oxygenic phototrophic organisms (algae and photosynthetic purple sulfur bacteria), adopted the Calvin-Benson cycle for CO_2 fixation, which preferentially used CO_2 rich in ^{12}C to synthesize organic matter and thus led to an enriched ^{12}C in the organic organism (Jia et al., 2007). As a result, the compound-specific $\delta^{13}C$ of ATMBs derived from GSB was usually much heavier than lipids (concomitant *n*-alkanes) derived from other oxygenic phototrophic organisms. The former ranged from −24.7‰ to −15.6‰ (or > −25‰) (Table 1) as summarized by previous works (Summons and Powell, 1986; Hartgers et al., 1994a, b; Koopmans et al., 1996a; Grice et al., 1997; Pedentchouk et al., 2004), which was 12–15‰ heavier than the latter. Thus, the $\delta^{13}C$ of compound-specific ATMBs was considered as the only identification mark to distinguish the source of GSB from other biological organisms (Koopmans et al., 1996b). But the compound-specific $\delta^{13}C$ of ATMBs within the source rock extracts could not be directly measured due to the extremely low abundance in the complex aromatic fraction mixtures, which is still an international challenge as suggested by previous studies (Koopmans et al., 1996b). Based on the facts that (1) the abundant crude oils from the Lower Paleozoic were contributed by the Middle-Upper Ordovician and/or Cambrian-Lower Ordovician source rocks; (2) the ATMBs were detected in all above oils; and (3) the ATMBs were only identified in $\epsilon_1 y$ source rocks from the Lower Paleozoic strata near the above oil areas, it

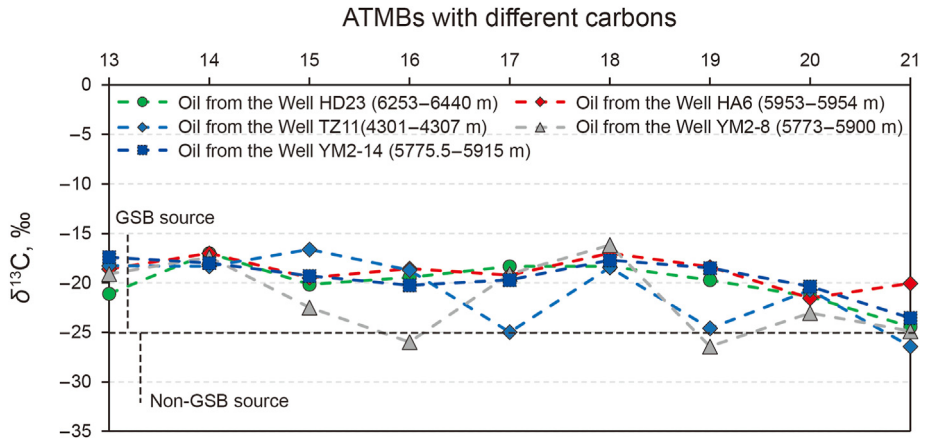


Fig. 4. Compound specific $\delta^{13}C$ of ATMBs in typical crude oils (GSB, green sulfur bacteria).

was believed that the ATMBs from the $\epsilon_1 y$ source rocks had the same precursor as that identified in the Lower Paleozoic crude oil (Huang et al., 2016; He et al., 2022a). Representative crude oil samples with abundant ATMBs from the most oil-rich structural belts, Tazhong Uplift and Tabei Uplift, were carried out for compound-specific $\delta^{13}C$ of ATMBs. Results show that the $\delta^{13}C$ values ranged from −24.87‰ to −16.17‰, which was all heavier than −25‰ with the heaviest value of −16.17‰, and was about 15‰ heavier than that of lipids (concomitant *n*-alkanes) of algae or other photosynthetic bacteria (Table 3 and 4, Fig. 4). These values were comparable with the published compound-specific $\delta^{13}C$ of ATMBs from the GSB, revealing that the investigated ATMBs from crude oil and $\epsilon_1 y$ source rocks were all derived from the GSB rather than other biological precursors.

The GSB is a strictly anaerobic photoautotroph using reduced sulfur compounds (e.g., H_2S, HS^-) as electron donors for photosynthesis and is only developed in the PZE condition (Peters et al., 2005; Grice et al., 2005; Júnior et al., 2013; Melendez et al., 2013; Spaak et al., 2018). It means that these source rocks containing abundant ATMBs derived from GSB should be developed under anoxia and euxinic conditions, as evidenced by our previous works with inorganic geochemical data (He et al., 2020b, 2022a) and predominant thiofluorene abundance in the trifluorene series (SF, thiofluorene; OF, oxyfluorene; F, fluorene). Multiple inorganic geochemical evidence, including V/(V+Ni)>0.8 (clear to 1 for siliceous shale), U/Th>4 (up to 45), and the enrichment factors plot of Mo & U element, suggested that hydrothermal activity triggered a benthic anoxic to H_2S-rich/euxinic condition during the early Cambrian, which remarkably enhanced the preservation of buried organic matter from the $\epsilon_1 y$ source rocks with TOC up to 29.8% (He et al., 2020b, 2022a; Zhu et al., 2021). Additionally, SF, OF and F might be derived from the same source. F will be converted to OF in the sub-oxidizing to sub-reducing conditions; while it will be converted to SF by replacing the chemically active α carbon atoms on position 9 of F by reduced sulfur atoms, in the reducing-anoxic environment (Xu et al., 2020). SF would have a dominant content in the H_2S-rich/euxinic condition because of the ample availability of reduced S elements. Results of trifluorene series from the Lower Paleozoic source rocks showed that SF% {SF% = SF/(SF+OF+F)* 100%)} from the $\epsilon_1 y$ source rocks had the highest content, ranging from 80% to 98% (Suppl. Fig. S3), which were two times higher than that from other source rocks in the Tarim Basin and that from the delta front shale (SF% = 41.56%) and deep lake shale (SF% = 21.19%) developed under reducing conditions (Xu et al., 2020). Therefore, the $\epsilon_1 y$ source rocks were developed under euxinic conditions, indicating that the ample reduced S element (H_2S) was available and promoted the formation of PZE, as well as the bloom of GSB during the early Cambrian in the Tarim Basin.

5.3. Implications for the oil-source correlation

Abundant Lower Paleozoic deep crude oil from the Tarim Basin has experienced a complex process of hydrocarbon accumulation, including multi-stage secondary alterations (especially TSR), multi-stage adjustments, and multi-stage accumulations. This complex process led to the limited effectiveness of traditional steroid/terpenoid biomarkers that were widely used in the oil-source correlations. Traditional steroid/terpenoid/aromatic biomarker indicators {such as Pr/Ph, dinostane, rearranged sterane/regular sterane, C_{28} St, C_{28} triaromatic steranes (C_{28} TAS), METAS and Ts/(Ts+Tm)} suggested that most of the crude oils from the Tabei Uplift and Tazhong Uplift were contributed by the Middle-Upper Ordovician source rocks (Huang et al., 2016). Especially, among the Lower Paleozoic source rocks, only the $O_3 l$ source rocks had extremely abundant C_{28} TAS and METAS, which showed an obvious genetic relationship to the most above crude oils. This could be typically reflected by the oil-source correlation from the well TZ30 (~5000 m, $O_3 l$) (Suppl. Figs. S4c–f). According to the traditional idea of oil-source correlation, it seemed that these crude oils might come from the contribution of $O_3 l$ source rocks. While, the distributions of C_{28}TAS and METAS in the oil inclusion from the well TZ30 (~5014 m, $O_3 l$) showed the opposite characteristics to that of the above in-situ crude oil (Suppl. Figs. S4a–f). Besides, the crude oil from above well TZ30 (~5000 m, $O_3 l$) contained abundant diagnostic biomarkers of ATMBs that were only developed in the $\epsilon_1 y$ source rocks and were not observed in the $O_3 l$ source rocks within the Lower Paleozoic (Suppl. Fig. S4g, h). It suggested that these crude oils might also have contributions from the $\epsilon_1 y$ source rocks rather than only from the $O_3 l$ source rocks.

Because of a few deep exploration wells drilled to the ϵ_1y and the limitations of detection methods, the existence of source rocks containing abundant ATMBs was once just a speculation that there was at least one other source kitchen developed under the PZE conditions and served as an important contributor in the Lower Paleozoic petroleum systems, since the abundant ATMBs from the Lower Paleozoic deep crude oils were detected for the first time (Sun et al., 2003). With the increasing depth and the number of new exploration wells (such as the Well LT1, Well LT3 and QT1), ATMBs were detected in $\epsilon_1 y$ source rocks (those from well LT1, $\epsilon_1 y$, 8654.39 m; well LT3, $\epsilon_1 y$, 8518.3 m; well QT1, $\epsilon_1 y$, 5966.4 m; SARK

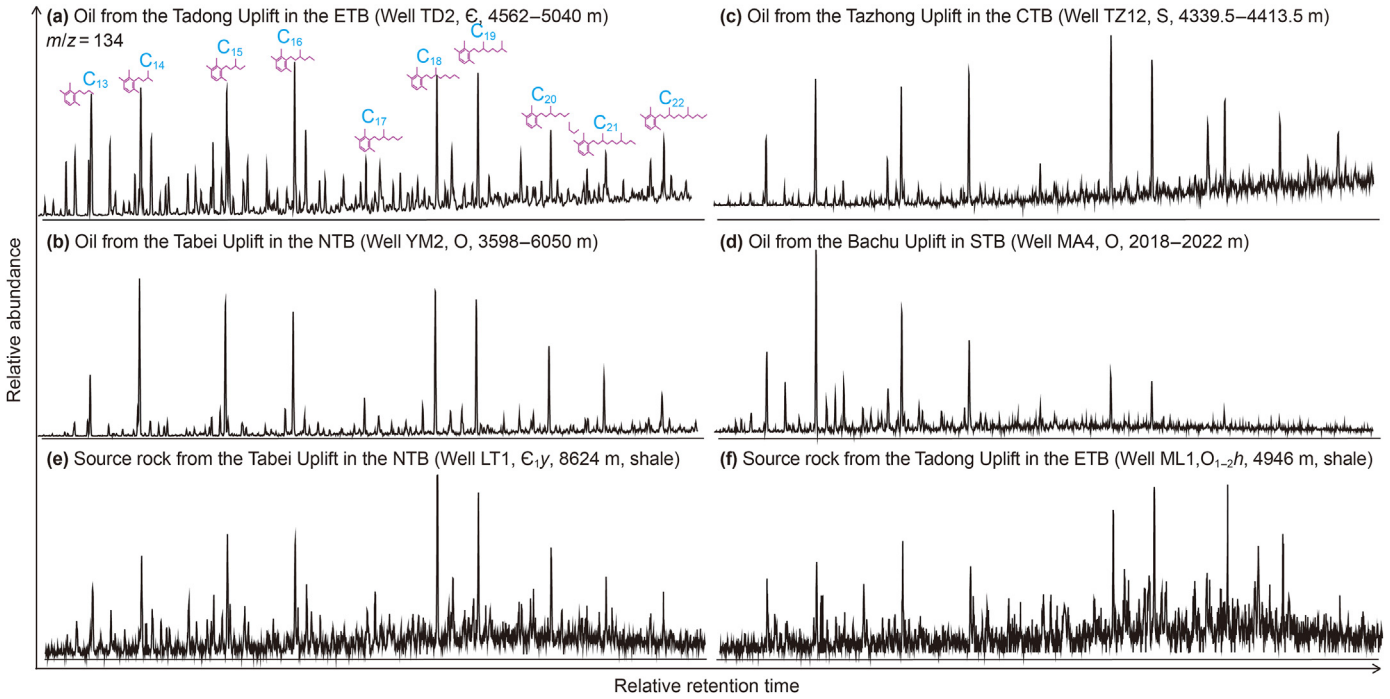


Fig. 5. A comparison of chromatograms of ATMBs (m/z = 134; ETB, eastern Tarim Basin; CTB, central Tarim Basin; NTB, northern Tarim Basin; STB, southern Tarim Basin).

section, $Є_1y$, outcrop) in this study, which revealed the existence of source rocks developed under the PZE conditions by the support of $\delta^{13}C$ values of ATMBs. Additionally, considering the strong anti-second-alteration abilities of ATMBs discussed above, the oil-source correlation based on ATMBs between $Є_1y$ source rocks and typical crude oils from Tazhong Uplift, Tabei Uplift, and Bachu Uplift revealed that almost all marine crude oils in the Tarim Basin contained contributions from $Є_1y$ source rocks (Fig. 5).

Thus, these crude oils, characterized by abundant ATMBs, METAS, and C_{28} TAS from the Tazhong Uplift and Tabei Uplift, were mixed crude oils. The mixed-oil phenomenon was believed to be extremely common, which was evidenced by previous works (Li et al., 2010, 2015; Pang et al., 2016) and the oil-source correlations by discriminant analysis on above stable aromatic indicators including the ATMBs, METAS, and C_{28} TAS (this will be discussed in another paper). Based on the difference from the distribution of biomarkers and their related compound-specific $\delta^{13}C$, we divided these mixed crude oils into three types: (1) mixed crude oils between non-biodegraded crude oil and non-biodegraded crude oils, such as those simultaneously containing complete *n*-alkane distribution and abundant 25-norhopanes (typical biodegradable product); (2) mixed crude oils from early-generated and late-generated crude oils, such as those displaying great differences between the current crude oil and the early-captured in-situ oil inclusion (Well TZ30, O_3l, ~5000 m; Suppl. Figs. S4a–d); (3) mixed crude oils from different source rocks, such as those simultaneously containing abundant ATMBs, C_{28} TAS, and METAS, as well as those had remarkable $\delta^{13}C$ difference (>5‰) on compound-specific *n*-alkane from current oil and in-situ oil inclusion (Well TZ421, O, 3221–3281 m, Suppl. Fig. S5).

Quantitative de-convolution was performed for mixed crude oils in the Tazhong Uplift based on the carbon isotope balance model (Pang et al., 2016). The calculated contribution from the $Є_1y$ source rocks to the mixed crude oil was dominantly higher than 50%, and about 60%–70% contribution to those mixed crude oils within areas less than 5 km from oil-source faults (Pang et al., 2016). This result was more refined than the traditional understanding of crude oil sources that were vaguely believed to be the Є-O_1 and/or O_{2-3} source rocks (Huang et al., 2016). And it was consistent with the widespread distribution of organic-rich source rocks from the $Є_1y$ (Zhu et al., 2018b) and limited distribution of O_{2-3} source rocks (mainly the Middle-Upper Ordovician marls) that were only developed in the margins of the structural uplifts (Sun et al., 2003).

Therefore, the ATMBs, as diagnostic biomarkers derived from GSB surviving under PZE conditions, could play a significant role in revealing the origin of Lower Paleozoic deep crude oil in the Tarim Basin. According to the strong anti-secondary-alteration ability and the unequivocal precursor under special habitat conditions, ATMBs would promote the targeted exploration in similar petroliferous basins or depressions with abundant deep crude oil resources or severe-secondary-altered crude oil resources, such as the Nyurol'ka Depression, southeastern Western Siberia plate (Chirkova et al., 2017); Northern Alberta, Canada (Bennett and Jiang, 2021); the Ardmore Basin, Oklahoma (Philp and DeGarmo, 2020); Western Canada and the Williston Basins (Requejo et al., 1992).

6. Conclusion

Composition and compound-specific $\delta^{13}C$ analysis of ATMBs were performed on crude oil from the Tarim Basin for the first time. The heavier compound-specific $\delta^{13}C$ values (up to −16‰) of ATMBs indicated a biological source of GSB, and thus, a PZE environment during the deposition of the corresponding source rocks is proposed. The existence of ATMBs in the $Є_1y$, $O_{1-2}h$ source rocks and crude oils with different alterations from the Lower Paleozoic indicated high stability for the ATMBs to multiple secondary alterations. It was suggested that the $Є_1y$ and $O_{1-2}h$ source rocks were developed under PZE conditions that triggered the significant enrichment of organic matter, which was supported by organic and inorganic geochemical data in our studies. Additionally, oil-source correlation results suggested that the ATMBs would provide

important insights for exploration of deep crude oils and severe secondary-altered crude oils in the Tarim Basin, due to their indication of the unequivocal precursor (GSB) under special habitat conditions (PZE).

Authors' contributions

Tao-Hua He, Conceptualization and writing the original draft; Wen-Hao Li and Shuang-Fang Lu, Supervision and Conceptualization; Er-Qiang Yang and Tao-Tao Jing, Software and Methodology; Jun-Feng Ying and Peng-Fei Zhu, Investigation; Xiu-Zhe Wang and Zhong-Hong Chen, Writing—Review & Editing; Wen-Qing Pan, Resources. All authors commented on the previous version and approved the final version of this manuscript.

Availability of data and material

Detailed information describing the experimental data is in the main text.

Declaration of competing interest

We confirm that there are no known conflicts of interest associated with this publication and there has been no significant financial support for this work that could have influenced its outcome. We confirm that the manuscript has been read and approved by all named authors and that there are no other persons who satisfied the criteria for authorship but are not listed. We further confirm that the order of authors listed in the manuscript has been approved by all of us. We confirm that we have given due consideration to the protection of intellectual property associated with this work and that there are no impediments to publication, including the timing of publication, with respect to intellectual property. In so doing we confirm that we have followed the regulations of our institutions concerning intellectual property.

Acknowledgments

The authors are grateful for the financial support provided by the National Science and Technology Major Project of the Ministry of Science and Technology of China (2016ZX04004-004), National Natural Science Foundation of China (41672125). We also appreciate Petroleum Exploration & Production Research Institute, Tarim Oilfield Company for arranging access to the oil and source rocks and providing some geochemical data. And special thanks are given to A-Prof. Qilin Xiao from the Key Laboratory of Oil and Gas Resources and Exploration Technology, Yangtze University, Wuhan, for his help in 2-thiadiamondoids analysis. Besides, we thank anonymous reviewers for their helpful comments and suggestions which improved the manuscript.

Appendix A. Supplementary data

Supplementary data to this article can be found online at https://doi.org/10.1016/j.petsci.2022.07.014.

References

Bennett, B., Jiang, C.Q., 2021. Oil-source and oil-oil correlations and the origin of the heavy oil and bitumen accumulations in Northern Alberta, Canada. Org. Geochem. 153, 104119. https://doi.org/10.1016/j.orggeochem.2021.104199.

Brocks, J.J., Schaeffer, P., 2008. Okenane, a biomarker for purple sulfur bacteria (Chromatiaceae), and other new carotenoid derivatives from the 1640 Ma Barney Creek Formation. Geochem. Cosmochim. Acta 72 (5), 1396–1414. https://doi.org/10.1016/j.gca.2007.12.006.

Cai, C.F., Li, K.K., Ma, A.L., et al., 2009. Distinguishing Cambrian from Upper Ordovician source rocks: evidence from sulfur isotopes and biomarkers in the Tarim Basin. Org. Geochem. 40 (7), 755–768. https://doi.org/10.1016/j.orggeochem.2009.04.008.

Cai, C.F., Zhang, C.M., Worden, R.H., et al., 2015. Application of sulfur and carbon isotopes to oil-source rock correlation: a case study from the Tazhong area. Tarim Basin, China. Org. Geochem. 83–84, 140–152. https://doi.org/10.1016/j.orggeochem.2015.03.012.

Cai, C.F., Amrani, A., Worden, R.H., et al., 2016. Sulfur isotopic compositions of individual organosulfur compounds and their genetic links in the lower paleozoic petroleum pools of the Tarim Basin, NW China. Geochem. Cosmochim. Acta 182 (1), 88–108. https://doi.org/10.1016/j.gca.2016.02.036.

Chen, Z.H., Wang, T.G., Li, M.J., et al., 2018. Biomarker geochemistry of crude oils and Lower Paleozoic source rocks in the Tarim Basin, western China: an oil-source rock correlation study. Mar. Petrol. Geol. 96, 94–112. https://doi.org/10.1016/j.marpetgeo.2018.05.023.

Chirkova, D.Y., Krasnoyarova, N.A., Serebrennikova, O.V., et al., 2017. Aryl isoprenoids in crude oils of the Nyurol'ka depression (southeast of Western Siberia). Petrol. Chem. 57 (1), 54–59. https://doi.org/10.1134/S0965544116090036.

Grice, K., Schaeffer, P., Schwark, L., et al., 1997. Changes in palaeoenvironmental conditions during deposition of the Permian Kupferschiefer (Low Rhine Basin, northwest Germany) inferred from molecular and isotopic compositions of biomarker components. Org. Geochem. 26 (11), 677–690. https://doi.org/10.1016/S0146-6380(97)00036-3.

Grice, K., Cao, C.Q., Love, G.D., et al., 2005. Photic zone euxinia during the Permian-Triassic superanoxic event. Science 307 (5710), 706–709. https://doi.org/10.1126/science.1104323.

Hartgers, W.A., Sinninghe Damsté, J.S., Requejo, A.G., et al., 1994a. Evidence for only minor contributions from bacteria to sedimentary organic carbon. Nature 369 (6477), 224–227. https://doi.org/10.1038/369224a0.

Hartgers, W.A., Sinninghe Damsté, J.S., Requejo, A.G., et al., 1994b. A molecular and carbon isotopic study towards the origin and diagenetic fate of diaromatic carotenoids. Org. Geochem. 22 (3–5), 703–725. https://doi.org/10.1016/0146-6380(94)90134-1.

He, T.H., Lu, S.F., Li, W.H., et al., 2018. Effect of salinity on source rock formation and its control on the oil content in shales in the hetaoyuan formation from the biyang depression, nanxiang basin, Central China. Energy Fuel. 32 (6), 6698–6707. https://doi.org/10.1021/acs.energyfuels.8b01075.

He, T.H., Lu, S.F., Li, W.H., et al., 2020a. Geochemical characteristics and effectiveness of thick, black shales in southwestern depression. Tarim Basin. J. Petrol. Sci. Eng. 185, 106607. https://doi.org/10.1016/j.petrol.2019.106607.

He, T.H., Lu, S.F., Li, W.H., et al., 2020b. Paleoweathering, hydrothermal activity and organic matter enrichment during the formation of earliest Cambrian black strata in the northwest Tarim Basin, China. J. Petrol. Sci. Eng. 189, 106987. https://doi.org/10.1016/j.petrol.2020.106987.

He, T.H., Li, W.H., Lu, S.F., et al., 2022a. Mechanism and geological significance of anomalous negative $\delta^{13}C_{kerogen}$ in the lower cambrian, NW Tarim Basin, China. J. Petrol. Sci. Eng. 208, 109384. https://doi.org/10.1016/j.petrol.2021.109384.

He, T.H., Li, W.H., Lu, S.F., et al., 2022b. Quantitatively unmixing method for complex mixed oil based on its fractions carbon isotopes: a case from the Tarim Basin, NW China. Petrol. Sci. (in press).

Hu, T., Pang, X.Q., Jiang, F.J., et al., 2021. Movable oil content evaluation of lacustrine organic-rich shales: methods and a novel quantitative evaluation model. Earth Sci. Rev. 214, 103545. https://doi.org/10.1016/j.earscirev.2021.103545.

Huang, H.P., Zhang, S.C., Su, J., 2016. Palaeozoic oil-source correlation in the Tarim Basin, NW China: a review. Org. Geochem. 94, 32–46. https://doi.org/10.1016/j.orggeochem.2016.01.008.

Huang, H.P., Zhang, S.C., Gu, Y., et al., 2017. Impacts of source input and secondary alteration on the extended tricyclic terpane ratio: a case study from Palaeozoic sourced oils and condensates in the Tarim Basin, NW China. Org. Geochem. 112, 158–169. https://doi.org/10.1016/j.orggeochem.2017.07.012.

Jia, W.L., Peng, P.A., Yu, C.L., et al., 2007. Source of 1,2,3,4-tetramethylbenzene in asphaltenes from the Tarim Basin. J. Asian Earth Sci. 30 (5–6), 591–598. https://doi.org/10.1016/j.jseaes.2006.09.003.

Jiang, N.H., Zhu, G.Y., Zhang, S.C., et al., 2008. Detection of 2-thiaadamantanes in the oil from well TZ-83 in Tarim Basin and its geological implication. Chin. Sci. Bull. 53 (3), 396–401. https://doi.org/10.1007/s11434-008-0099-6.

Júnior, G.R.S., Santos, A., Lima, S.D., et al., 2013. Evidence for euphotic zone anoxia during the deposition of Aptian source rocks based on aryl isoprenoids in petroleum, Sergipe-Alagoas Basin, northeastern Brazil. Org. Geochem. 63 (1), 94–104. https://doi.org/10.1016/j.orggeochem.2013.07.009.

Koopmans, M.P., Köster, J., Van Kaam-Peters, H.M.E., et al., 1996a. Diagenetic and catagenetic products of isorenieratene: molecular indicators for photic zone anoxia. Geochem. Cosmochim. Acta 60 (22), 4467–4496. https://doi.org/10.1016/S0016-7037(96)00238-4.

Koopmans, M.P., Schouten, S., Kohnen, M.E., et al., 1996b. Restricted utility of aryl isoprenoids as indicators for photic zone anoxia. Geochem. Cosmochim. Acta 60 (23), 4873–4876. https://doi.org/10.1016/S0016-7037(96)00303-1.

Li, S.M., Pang, X.Q., Zhang, B.S., et al., 2010. Oil-source rock correlation and quantitative assessment of Ordovician mixed oils in the Tazhong Uplift, Tarim Basin. Petrol. Sci. 7 (2), 179–191. https://doi.org/10.1007/s12182-010-0025-9.

Li, S.M., Amrani, A., Pang, X.Q., et al., 2015. Origin and quantitative source assessment of deep oils in the Tazhong Uplift. Tarim Basin. Org. Geochem. 78, 1–22. https://doi.org/10.1016/j.orggeochem.2014.10.004.

Li, J.Z., Tao, X.W., Bai, B., et al., 2021. Geological conditions, reservoir evolution and favorable exploration directions of marine ultra-deep oil and gas in China.

Petrol. Explor. Dev. 48 (1), 60–79. https://doi.org/10.1016/S1876-3804(21)60005-8.
Li, M.P., Chen, Z.H., Yi, S.W., et al., 2022. Origin and accumulation mechanisms of deep paleozoic oil and gas: a case study of the central Tarim basin, western China. J. Petrol. Sci. Eng. 208, 109634. https://doi.org/10.1016/j.petrol.2021.109634.
Liu, C.G., Qi, L.X., Liu, Y.L., et al., 2016. Positive carbon isotope excursions: global correlation and genesis in the Middle–Upper Ordovician in the northern Tarim Basin, Northwest China. Petrol. Sci. 13 (2), 192–203. https://doi.org/10.1007/s12182-016-0096-3.
Liu, Y.C., Dong, S.Y., Zhao, C.H., 2021. Thermal evolution and the maturation of the deeply buried lower Paleozoic source rocks in the Tarim Basin, northwest China. Arabian J. Geosci. 14 (13), 1238. https://doi.org/10.1007/s12517-021-07562-w.
Lu, H., Shen, C.C., Zhang, Z.R., et al., 2015. 2,3,6-/2,3,4-aryl isoprenoids in Paleocene crude oils from Chinese Jianghan Basin: constrained by water column stratification. Energy Fuel. 29 (8), 4690–4700. https://doi.org/10.1021/acs.energyfuels.5b00110.
Ma, A.L., Jin, Z.J., Zhu, C.S., et al., 2018. Detection and significance of higher thiadiamondoids and diamondoidthiols in oil from the Zhongshen 1C well of the Tarim Basin, NW China. Sci. China Earth Sci. 61 (10), 1440–1450. https://doi.org/10.1007/s11430-017-9244-7.
Ma, Y.S., Cai, X.Y., Yun, L., et al., 2022. Practice and theoretical and technical progress in exploration and development of Shunbei ultra-deep carbonate oil and gas field, Tarim Basin, NW China. Petrol. Explor. Dev. 49 (1), 1–20. https://doi.org/10.1016/S1876-3804(22)60008-9.
Melendez, I., Grice, K., Trinajstic, K., et al., 2013. Biomarkers reveal the role of photic zone euxinia in exceptional fossil preservation: an organic geochemical perspective. Geology 41 (2), 123–126. https://doi.org/10.1130/G33492.1.
Pang, X.Q., Chen, J.Q., Li, S.M., et al., 2016. Evaluation method and application of the relative contribution of marine hydrocarbon source rocks in the Tarim Basin: a case study from the Tazhong area. Mar. Petrol. Geol. 77, 1–18. https://doi.org/10.1016/j.marpetgeo.2016.05.023.
Pedentchouk, N., Freeman, K.H., Harris, N.B., et al., 2004. Sources of alkylbenzenes in Lower Cretaceous lacustrine source rocks, West African rift basins. Org. Geochem. 35 (1), 33–45. https://doi.org/10.1016/j.orggeochem.2003.04.001.
Peters, K.E., Walters, C.C., Moldowan, J.M., 2005. The Biomarker Guide: Biomarkers and Isotopes in Petroleum Exploration and Earth History. Cambridge University Press, Cambridge, New York, Melborne.
Philp, R.P., DeGarmo, C.D., 2020. Geochemical characterization of the devonian-mississippian woodford shale from the McAlister cemetery quarry, criner hills uplift, Ardmore Basin. Oklahoma. Mar. Petrol. Geol. 112, 104078. https://doi.org/10.1016/j.marpetgeo.2019.104078.
Quandt, L., Gottschalk, G., Ziegler, H., et al., 1977. Isotope discrimination by photosynthetic bacteria. FEMS Microbiol. Lett. 1 (3), 125–128. https://doi.org/10.1111/j.1574-6968.1977.tb00596.x.
Requejo, A.G., Allan, J., Creaney, S., et al., 1992. Aryl isoprenoids and diaromatic carotenoids in Paleozoic source rocks and oils from the Western Canada and Williston Basins. Org. Geochem. 19 (1–3), 245–264. https://doi.org/10.1016/0146-6380(92)90041-U.
Sinninghe Damsté, J.S., Schouten, S., Van Duin, A.C.T., 2001. Isorenieratene derivatives in sediments: possible controls on their distribution. Geochem. Cosmochim. Acta 65 (10), 1557–1571. https://doi.org/10.1016/S0016-7037(01)00549-X.
Spaak, G., Edwards, D.S., Allen, H.J., et al., 2018. Extent and persistence of photic zone euxinia in Middle-Late Devonian seas - insights from the Canning Basin and implications for petroleum source rock formation. Mar. Petrol. Geol. 93, 33–56. https://doi.org/10.1016/j.marpetgeo.2018.02.033.
Summons, R.E., Powell, T.G., 1986. Chlorobiaceae in Paleozoic seas revealed by biological markers, isotopes and geology. Nature 319 (6056), 763–765. https://doi.org/10.1038/319763a0.
Summons, R.E., Powell, T.G., 1987. Identification of aryl isoprenoids in source rocks and crude oils: biological markers for the green sulphur bacteria. Geochem. Cosmochim. Acta 51 (3), 557–566. https://doi.org/10.1016/0016-7037(87)90069-X.
Sun, Y.G., Xu, S.P., Lu, H., et al., 2003. Source facies of the Paleozoic petroleum systems in the Tabei uplift, Tarim Basin, NW China: implications from aryl isoprenoids in crude oils. Org. Geochem. 34 (4), 629–634. https://doi.org/10.1016/S0146-6380(03)00063-9.
Sun, L.D., Zou, C.N., Zhu, R.K., et al., 2013. Formation, distribution and potential of deep hydrocarbon resources in China. Petrol. Explor. Dev. 40 (6), 687–695. https://doi.org/10.1016/S1876-3804(13)60093-2.
Wang, Q.R., Huang, H.P., Chen, H.H., et al., 2020. Secondary alteration of ancient Shuntuoguole oil reservoirs, Tarim Basin, NW China. Mar. Petrol. Geol. 111, 202–218. https://doi.org/10.1016/j.marpetgeo.2019.08.013.
Wei, Z., Walters, C.C., Moldowan, J.M., et al., 2012. Thiadiamondoids as proxies for the extent of thermochemical sulfate reduction. Org. Geochem. 44 (1), 53–70. https://doi.org/10.1016/j.orggeochem.2011.11.008.
Xiao, Q.L., Sun, Y.G., He, S., et al., 2019. Thermal stability of 2-thiadiamondoids determined by pyrolysis experiments in a closed system and its geochemical implications. Org. Geochem. 130, 14–21. https://doi.org/10.1016/j.orggeochem.2019.02.003.
Xu, Z.J., Liu, L.F., Jiang, S., et al., 2020. Palaeoenvironment and organic matter of the Triassic Chang 9 lacustrine shales, ordos basin, China. Geol. J. 55 (6), 4748–4771. https://doi.org/10.1002/gj.3706.
Yu, S., Pan, C.C., Wang, J.J., et al., 2011. Molecular correlation of crude oils and oil components from reservoir rocks in the Tazhong and Tabei uplifts of the Tarim Basin. China. Org. Geochem. 42 (10), 1241–1262. https://doi.org/10.1016/j.orggeochem.2011.08.002.
Zhan, Z.W., Zou, Y.R., Shi, J.T., et al., 2016. Unmixing of mixed oil using chemometrics. Org. Geochem. 92, 1–15. https://doi.org/10.1016/j.orggeochem.2015.11.006.
Zhang, Z.R., Volkman, J.K., Xie, X.M., et al., 2016. Stepwise pyrolysis of the kerogen from the Huadian oil shale, NE China: algaenan-derived hydrocarbons and mid-chain ketones. Org. Geochem. 91, 89–99. https://doi.org/10.1016/j.orggeochem.2015.10.011.
Zhou, X.Q., Chen, D.Z., Qing, H.R., et al., 2014. Submarine silica-rich hydrothermal activity during the earliest cambrian in the Tarim Basin, northwest China. Int. Geol. Rev. 56 (15), 1906–1918. https://doi.org/10.1080/00206814.2014.968885.
Zhu, G.Y., Milkov, A.V., Chen, F.R., et al., 2018a. Non-cracked oil in ultra-deep high-temperature reservoirs in the Tarim basin, China. Mar. Petrol. Geol. 89, 252–262. https://doi.org/10.1016/j.marpetgeo.2017.07.019.
Zhu, G.Y., Chen, F.R., Wang, M., et al., 2018b. Discovery of the lower Cambrian high-quality source rocks and deep oil and gas exploration potential in the Tarim Basin, China. AAPG Bull. 102 (10), 2123–2151. https://doi.org/10.1306/03141817183.
Zhu, G.Y., Li, J.F., Zhang, Z.Y., et al., 2020. Stability and cracking threshold depth of crude oil in 8000 m ultra-deep reservoir in the Tarim Basin. Fuel 282, 118777. https://doi.org/10.1016/j.fuel.2020.118777.
Zhu, G.Y., Milkov, A.V., Li, J.F., et al., 2021. Deepest oil in Asia: characteristics of petroleum system in the Tarim Basin, China. J. Petrol. Sci. Eng. 199 (4), 108246. https://doi.org/10.1016/j.petrol.2020.108246.